ACCURATE AND ROBUST ADAPTIVE HYPERBOLIC-PID CONTROL STRATEGY FOR A SERVO PNEUMATIC SYSTEM

K.N. Kamaludin[1], L. Abdullah[1], S.N.S. Salim[2] and A.S.N. Chairat[3]

[1]Fakulti Teknologi dan Kejuruteraan Industri dan Pembuatan,
Universiti Teknikal Malaysia Melaka, Hang Tuah Jaya, 76100 Durian Tunggal, Melaka, Malaysia

[2]Fakulti Teknologi dan Kejuruteraan Elektrik,
Universiti Teknikal Malaysia Melaka, Hang Tuah Jaya, 76100 Durian Tunggal, Melaka, Malaysia

[3]Department of Industrial Engineering, Institut Teknologi PLN,
Menara PLN, Jl. Lkr. Luar Barat, RT.1/RW.1, Duri Kosambi, Kecamatan Cengkareng, Daerah Khusus Ibukota Jakarta, Jakarta 11750, Indonesia

Corresponding Author's Email: lokman@utem.edu.my

Article History: Received 12 March 2025; Revised 22 July 2025; Accepted 7 August 2025

ABSTRACT: Robust trajectory tracking and precise positioning remain critical challenges in servo pneumatic actuator systems, particularly under varying external load conditions. Conventional PID controllers, while widely adopted, often struggle with nonlinearities and internal disturbances such as friction. This study presents a comparative analysis of three advanced control strategies—PID with static friction compensation (PID+F_{SS}), Nonlinear Hyperbolic PID with F_{SS} (NH-PID+F_{SS}), and Triple Nonlinear Hyperbolic PID integrated with Single-Input Fuzzy Logic and Generalized Maxwell Slip friction compensation (T-NPID+SIFLC+F_{GMS}). The controllers are evaluated on a 100 mm amplitude sinewave trajectory at 0.1 Hz under no loading (0 kg), 1 kg, 5 kg, and 9 kg external loads. Design validation is grounded in the asymptotic tracking region (ATR) framework, ensuring convergence of error to zero and stability. Performance is quantified using maximum tracking error (MTE) and root mean square error (RMSE). Experimental results demonstrate that T-NPID+SIFLC+F_{GMS} achieves superior tracking accuracy and robustness, with up to 48.84% improvement in the measured performance compared to baseline PID+F_{SS}. The findings affirm the efficacy of integrating adaptive fuzzy logic and advance nonlinear PID. Future work will explore the comparison of

the different friction compensation module (F_{GMS} and F_{SS}) effecting the control strategy.

KEYWORDS: *Servo Pneumatic Control; Nonlinear PID; Single-Input Fuzzy Logic; Robust Control; Adaptive Control*

1.0 INTRODUCTION

Pneumatic actuators have been widely adopted in various industrial applications, including manipulators, riveting machines, automotive systems, and pick-and-place equipment. Their appeal lies in their simplicity, cost-effectiveness, and minimal heat generation under continuous operation. These advantages have driven sustained research interest in enhancing the performance of pneumatic actuators [1], [2] . However, achieving high-precision control remains a formidable challenge due to the inherent nonlinearities of pneumatic systems. These include dead zones, air compressibility, low damping, and frictional forces, particularly internal friction between the actuator's seal and cylinder wall. As highlighted by [3], friction compensation has emerged as a dominant focus in pneumatic control research, underscoring its critical impact on trajectory tracking and positioning accuracy.

Over the years, various control strategies have been proposed to address these nonlinearities. Adaptive control techniques, introduced in the early 2000, offer real-time parameter estimation for time-varying systems. Despite their theoretical robustness, adaptive controllers are less prevalent in industrial settings due to their complexity and limited precision compared to PID- and SMC-based approaches. Adaptive robust control (ARC), an evolution of adaptive control, incorporates robustness criteria to enhance stability and accuracy, and has been successfully extended to pneumatic systems [4]. Sliding mode control (SMC), known for its resilience to disturbances, has also been applied to the friction compensation method [5], [6]. However, its reliance on precise modelling and susceptibility to chattering limit its industrial viability. In contrast, PID-based strategies—especially those augmented with nonlinear or intelligent components—offer a more practical and

tuneable solution[7], [8]. These include multi-rate nonlinear PID (MN-PID), self-regulating nonlinear PID (SN-PID) [9], and double nonlinear PI controllers [10]. Excluding the author, no nonlinear PIDs adopting nonlinear functions and via friction compensation have been applied, therefore presenting a research gap. This study advances the T-NPID framework by incorporating a simplified yet effective fuzzy logic enhancement; The Single Input Fuzzy Logic (SIFLC) controller. The SIFLC approach streamlines the fuzzy inference process by utilizing a single input variable—typically derived from sliding mode signals or error dynamics—thereby reducing computational complexity while maintaining control efficacy. As reviewed by [11], certain types of SIFLC have been applied in pneumatic applications. The researchers employ Takagi–Sugeno (T-S) or Mamdani inference models with triangular or Gaussian membership functions. To date, the novel structure of the SIFLC by [11] has never been adopted in a servo pneumatic control strategy, owing to this reason, the T-NPID integrating the designated SIFLC (T-NPID+SIFLC) is explored in this research paper.

The remainder of this paper is structured as follows: Section 2 details the methodology for analysing the proposed control strategy using the Lyapunov's asymptotic tracking behaviour. Section 3 explains the controller design and Section 4 presents the experimental results and discussion. Finally, Section 5 concludes the study and outlines potential directions for future research.

2.0 METHODOLOGY

2.1 System setup and modelling

The servo pneumatic actuator system is modelled via a time-domain system identification approach. Figure 1 and Table 1 illustrate the experimental configuration and the apparatus employed. The actuator system interfaces with the personal computer (PC) through MATLAB using a peripheral component interconnect (PCI) card and data acquisition (DAQ) box. Modelling obtained via the System Identification (SI) toolbox in MATLAB yields the state-space model expressions in Equations 1 to 4. Conversion of the state-space to a

linearised transfer function is as presented in Equation 5.

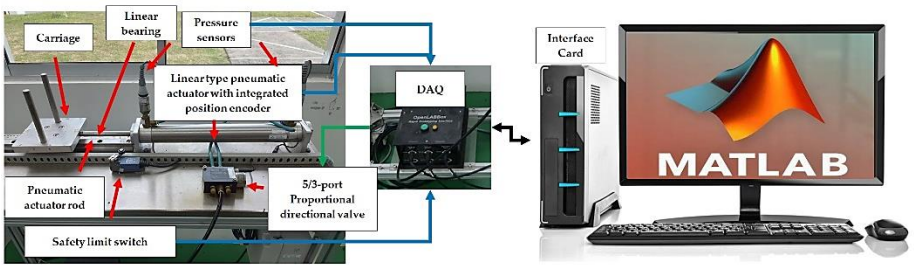

Figure 1: Experimental setup of the servo pneumatic system

Table 1: Experimental plant equipment list

Equipment	Model number	Specification
Proportional valve	Enfield LS-V15s	5/3 port, 0-10 Volts
Pneumatic actuator with integrated position encoder	Enfield ACTB-200-S10200	Double acting, 12 inch/ 304.80 mm stroke length
Pressure sensor	Gems Sensor 1200SGG	0 to 10 volts, 0-150 PSI
Safety limit switch	Tezuo AZ8104	Contact on
DAQ Box	National Instrument PCI-6221	37 Pin PCI
Matlab / SIMULINK	Version 2016b	N/A

$$\mathbf{A} = \begin{bmatrix} \mathbf{-0.2921} & \mathbf{-0.02056} & \mathbf{-0.000085} \\ \mathbf{1} & \mathbf{0} & \mathbf{0} \\ \mathbf{0} & \mathbf{1} & \mathbf{0} \end{bmatrix} \mathbf{B} = \begin{bmatrix} \mathbf{1} \\ \mathbf{0} \\ \mathbf{0} \end{bmatrix} \quad (1)$$

$$\mathbf{C} = [\mathbf{0.03468} \quad \mathbf{0.1468} \quad \mathbf{-0.002041}] \; \mathbf{D} = [\mathbf{0}] \quad (2)$$

$$\mathbf{x} = \mathbf{Ax} + \mathbf{Bu} \quad (3)$$

$$\mathbf{y} = \mathbf{Cx} + \mathbf{Du} \quad (4)$$

A are the state vectors, *B* is the measured output, *C* are the measured input and *D* is noise.

$$G(s) = \frac{0.03468s^2 + 0.1468s - 0.002041}{s^3 + 0.2921s^2 + 0.02056s + 0.000085} \quad (5)$$

3.0 CONTROLLER DESIGN: NONLINEAR HYPERBOLIC PID CONTROLLERS

Three controllers are compared to with the classical PID controller as reference. All the controllers in comparison are based on the classical PID controller. Th PID algorithm is presented in Equation 5, and the schematic of the PID with the plant's transfer function is illustrated in Figure 2(a). NH-PID adapts a nonlinear hyperbolic function in the

strategy in Figure 2 (b), and the function stated in Equation 6 [12]. T-NPID+SIFLC is based on the T-NPID controller [13], but with an additional SIFLC module, as shown in Figure 2(c). Since the research employs a friction compensation method, a static friction compensation feedback module (F_{SS}) is adapted to the two-base control strategy. The proposed control strategy, in turn, utilizes the Generalized Maxwell Slip (GMS) friction compensation module, as previously researched (F_{GMS}) [12] .

The nonlinear functions of the T-NPID are stated in Equations 7 to 9. Equation 10 presents the error algorithm for all of the nonlinear hyperbolic calculations. The tuned PID parameters are tabulated in Table 2. Extensions to the PID parameters, which include all the nonlinear hyperbolic parameters that were tuned heuristically and stochastically optimized using particle swarm optimization (PSO) [14], are tabulated in Tables 3 and 4.

$$G_{PID}(s) = K_P + \frac{K_I}{s} + K_D s \tag{5}$$

Table 2: Parameters of the PID

PID Parameter	
Parameter	Value
K_P	10
K_I	0.005
K_D	0.5

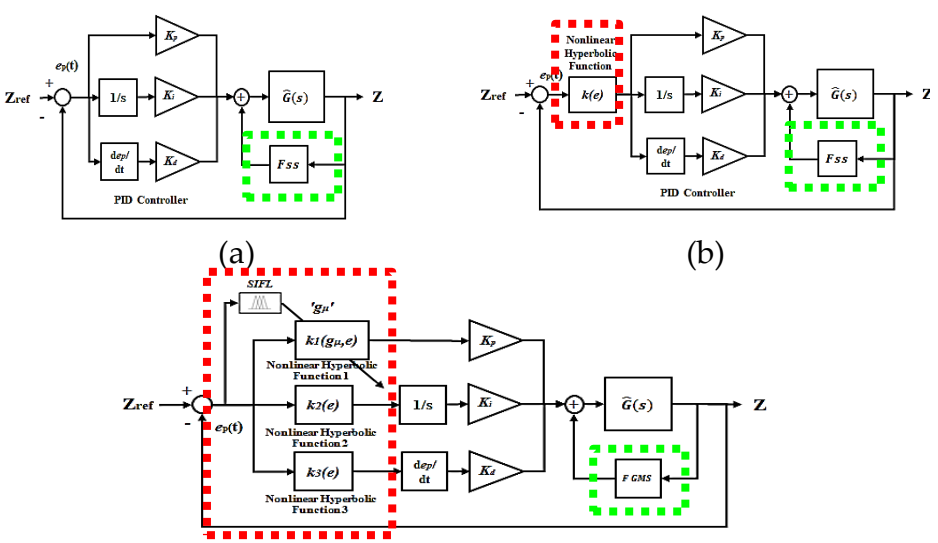

(c)

Figure 2: Schematic diagrams of the control strategy (a) PID+F_{SS}, (b) NH-PID+F_{SS}, and (c) T-NPID+SIFLC+F_{GMS}

$$K(e) = 1 + x \times [1 - \text{sech}(y \times e)] \quad (6)$$

$$K_P(e) = 1 + f \times [1 - \text{sech}(g \times e)] \quad (7)$$

$$K_I(e) = 1 \div [p + q \times (1 - \text{sech}(r \times e))] \quad (8)$$

$$K_D(e) = 1 \div [a + b \times (1 - \text{sech}(c \times e))] \quad (9)$$

$$\text{error}, e = \begin{cases} e, & |e| \leq e_{max} \\ e_{max} \cdot (\text{sign}(e)), & |e| > e_{max} \end{cases} \quad (10)$$

Table 3: Parameters of the NH-PID

Parameter	Value
x	9.450
y	3.050
e_{max}	0.5

Table 4: Parameters of the T-NPID

Parameter	Value
f	3.042
g	9.045
p	1
q	33.200
r	34.000
a	1
b	9.867
c	6.333
e_{max} P, I, D	0.5

Designing of the T-NPID+SIFLC integrates SIFLC as a control mechanism to vary one of the parameters in the nonlinear function. The integration improves the controller's flexibility and provides several gain changes [9]. For the $K_P(e)$, two parameters are available for rate variation, f and g. g is selected to be in line with the previous concept.

Fuzzy logic is able to be initially designed linguistically. The linguistic expression of the system's error range is expressed as Equation 11 and Equation 13, for all of the membership functions α as Equation 12 and Equation 14 show. The error range is set from zero (0) to one (1), whereas

the output of the fuzzy logic system is set from zero (0) to negative one (-1).

$$|\mathbf{e_x}| \in \{|\mathbf{e_1}|, |\mathbf{e_2}|, |\mathbf{e_3}|, \ldots\ldots |\mathbf{e_n}|, \} \tag{11}$$

$$\boldsymbol{\alpha_x} \in \{\boldsymbol{\alpha_1}, \boldsymbol{\alpha_2}, \boldsymbol{\alpha_3}, \ldots\ldots \Delta|\boldsymbol{\alpha_n}|\} \tag{12}$$

$$\mathbf{e} = \{\mathbf{e_x}|\mathbf{e_x} \rightarrow [\mathbf{0}, \mathbf{1}]\forall_{\mathbf{x}} = \mathbf{0}, \ldots\ldots \mathbf{1}\} \tag{13}$$

$$\boldsymbol{\alpha} = \{\boldsymbol{\alpha_x}|\boldsymbol{\alpha_x} \rightarrow [\mathbf{0}, -\mathbf{1}]\forall_{\boldsymbol{x}} = \mathbf{0}, \ldots\ldots -\mathbf{1}\} \tag{14}$$

The conversion of fuzzy logic to single-input fuzzy logic applies to the research by [15]. Commonly for a dual input fuzzy logic input is error *e*, and the error rate, Δe. The main advantage of SIFLC compared to standard fuzzy logic is the dismissal of the membership function of (Δe). Δe is converted into switching function s_1, as Equation 15 and Equation 17 shows. The aggressiveness of the relationship between *e* and Δe is tuned by λ. The membership functions (MFs) are able to be drastically reduced from 49 sets (α^2) to only 7 sets(α). The SIFLC MFs are tabulated in Table 5.

$$\mathbf{s_1} = \Delta\mathbf{e_n} + \boldsymbol{\lambda}\mathbf{e_n} \tag{15}$$

$$\mathbf{d_1} = \left[(\mathbf{e_n} - \mathbf{e_{n+1}})^2 + (\Delta\mathbf{e_n} - \Delta\mathbf{e_{n+1}})^2\right]^{\frac{1}{2}} \tag{16}$$

$$\mathbf{d_1} = \frac{|\dot{\mathbf{e}}_1 + \boldsymbol{\lambda}\mathbf{e_1}|}{\sqrt{\mathbf{1}+\boldsymbol{\lambda}^2}} \tag{17}$$

Table 5: SIFLC input and output MF function values

Input, e	LNB	LS1	LS2	LM	LB1	LB2	LB3
MF value	1, 0.15	0.05, 0.20, 0.35	0.20, 0.35, 0.50	0.35, 0.50, 0.65	0.50, 0.65, 0.80	0.65, 0.80, 0.95	0.85, 1
Output, α	Z	S1	S2	M	B1	B2	B3
MF Value	0	-0.167	-0.334	-0.5	-0.667	-0.834	-1

Designing the the symmetrical SIFLC follows the research by [16]. A rule table based on the input (error) of the system is created as tabulated in Table 6. The output membership function is a Sugeno type. All the MF's are spread symmetrically, hence the name symmetrical SIFLC. The control surface in Figure 3 shows the SIFLC relation between the input and output, and the whole figure is known as the piecewise linear function (PWL). According to Salam et al., [17], SIFLC is able to reduce calculation time. Consolidating the claim of computational savings, the C code (.c) generated via Simulink Coder yielded a 34.38% reduction in logic lines for the SIFLC controller compared to classical fuzzy logic (273 versus 416 lines). The corresponding header files (.h) also saw a 7.04% reduction. The reduction for both programming logic lines aligns with the reduction of fuzzy rules from 49 to 7 and confirms the structural simplicity of the single-input fuzzy logic design.

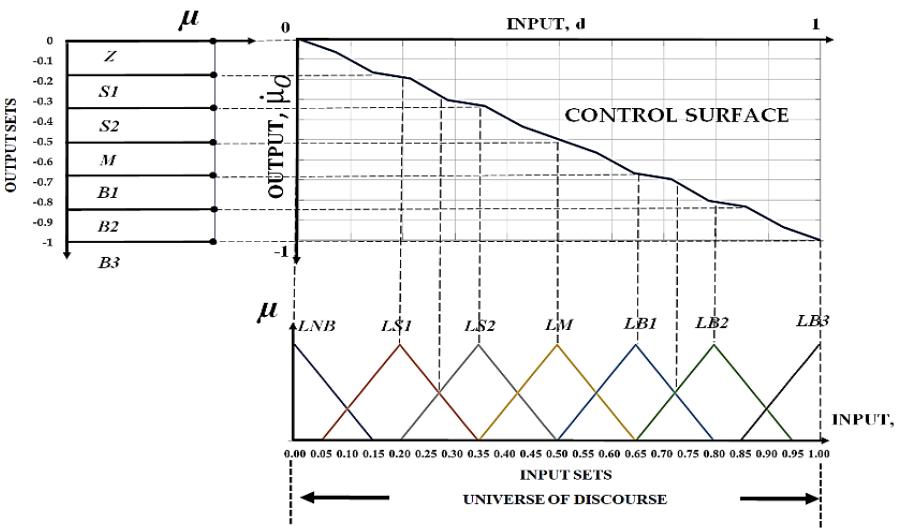

Figure 3: Control surface and PWL from the SIFLC MF

A simple adaptation formula is adapted within the SIFLC module to cater the simplicity of tuning the control strategy. The input of the SIFLC adapts Equation 14, from the systems error, e. The output of the SIFLC is adapted by Equation 15. Adapting Equation 14 and 15, allows the tuning to be performed without having to

constantly adjusting the fuzzy logic membership function, reducing setup complexity [9].

$$\mathbf{e_n} = \begin{cases} \frac{\mathbf{e_{volt}}}{\mathbf{e_{max}}} \cdot (\mathbf{Max}|\mathbf{e_x}|), & \mathbf{e} \leq \mathbf{e_{max}} \\ \mathbf{e_{max}} \cdot (\mathbf{Max}|\mathbf{e_x}|), & \mathbf{e} > \mathbf{e_{max}} \end{cases} \quad (14)$$

$$\mathbf{Adaptive\ g_{SIFLC}} = \mathbf{g_{min}} + [(\mathbf{g} - \mathbf{g_{min}}) \cdot \boldsymbol{\alpha}] \quad (15)$$

Figure 4 shows the full nonlinear function of the T-NPID with SIFLC. By observing the blue lines from the $K_P(e)$, there are multiple lines due to the *Adaptive* g_{SIFLC}. The *Adaptive* g_{SIFLC} adapts accordingly to the errors, allowing the the nonlinear function to vary between the minimum blue line (most bottom) and the maximum blue line (most top). The $K_I(e)$ and $K_D(e)$ are presented as the dark purple and dark red line, respectively.

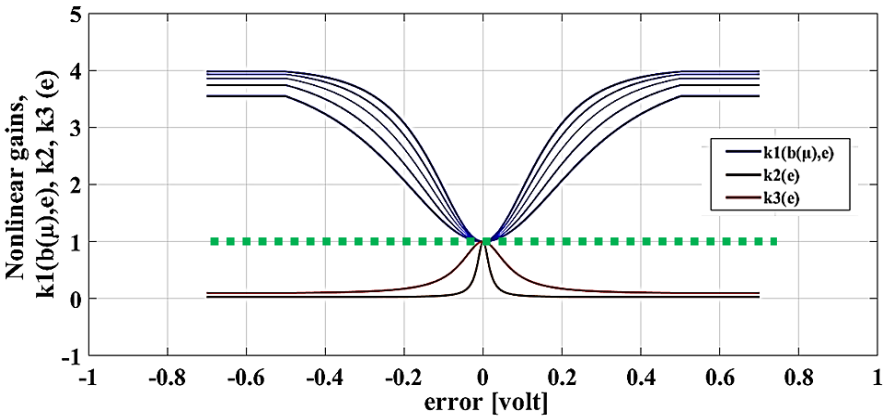

Figure 4: T-NPID+SIFLC nonlinear hyperbolic functions

3.1 Lyapunov's asymptotic tracking behaviour analysis

The tracking behaviour of a control strategy on a system is able to be predicted via the Lyapunov asymptotic analysis. Two types of analysis are able to be performed; the direct method and an indirect method. Since modelling of the pneumatic system has been linearised as a transfer function, the indirect method suits the analysis. To add to the factor, the indirect method does not require the full system knowledge [18]. The Lyapunov indirect method assesses local stability of nonlinear systems via linearisation. Consider the system:

$$\dot{x} = f(x, t), \text{where } f(0, t) = 0, \text{for all } t \geq 0 \quad (16)$$

Linearisation at the origin yields the Jacobian:

$$A(t) = \frac{\partial f(x,t)}{\partial x}\Big|_{x=0} \tag{17}$$

The residual terms:

$$f_1(x,t) = f(x,t) - A(t)x \tag{18}$$

Equation 18 approaches zero as $x \to 0$, but uniform convergence requires:

$$\lim_{||x||\to\infty} sup_{t\geq 0} \frac{||f_1(x,t)||}{||x||} = 0 \tag{19}$$

If satisfied, the linearised system:

$$z = \dot{A}(t)z \tag{20}$$

Equation 20 is uniformly asymptotically stable, implying local stability of the original nonlinear system. For time-invariant systems, stability is guaranteed if all eigenvalues of A lie in the open left-half of the complex plane. Applying this to the proposed plant (neglecting time delay), the closed-loop matrix is

$$A_{ClosedLoop} = A - B \cdot K \tag{21}$$

with the PID gains:

$$K = [10 \quad 0.5 \quad 0.005] \tag{22}$$

$\therefore$ where A and B follows Equation 1. Eigenvalues are computed via:

$$\det([A\_ClosedLoop] - \lambda I) = 0 \tag{23}$$

Table 6 summarises eigenvalues for PID, NH-PID, and T-NPID+SIFLC controllers. The eigenvalues are able to be represented as poles location on the pole-zero map (PZ-map). The pole-zero map as shown in Figure 5 shows that all poles lie on the negative side of the real axis, confirming asymptotic stability. The figure also illustrates that the nonlinear controllers (NH-PID and T-NPID+SIFLC) yield faster convergence and reduced oscillation due to larger negative real parts, and smaller imaginary components[19]. T-NPID+SIFLC have minimum and maximum eigenvalues due to the variable parameter of the mathematical function.

Table 6: Eigenvalues for all the control strategies

λ	Λ for PID	Λ for NH-PID	Λ for T-NPID+SIFLC	
			Max	Min
λ_1	-10.2562	-43.3419	-40.0419	-35.7408
λ_2	-0.0179 +0.0481i	-0.0176 +0.0471i	-0.0046 +0.0069i	-0.0052 +0.0071i
λ_3	-0.0179 -0.0481i	-0.0176 -0.0471i	-0.0046 -0.0069i	-0.0052 -0.0071i

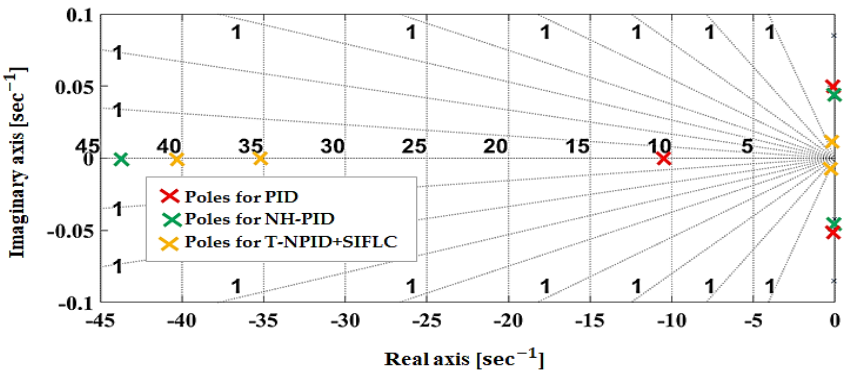

Figure 5: Poles of each control strategy

4.0 RESULT AND DISCUSSION

A sinusoidal wave of 0.1 Hz and an amplitude of 100 mm is used as the desired trajectory. The runs were performed for 100 seconds, and the error data were recorded for 100 seconds from t=50 seconds. Three types of controllers were compared for performance evaluation: the classical PID+FSS, NH-PID+F_{SS}, and the novel T-NPID+SIFLC+F_{GMS}.

Two performance measures were taken for all the controllers: the maximum tracking error, MTE, and root mean square error, RMSE, as Equations 16 and 17 show accordingly. The simulation results for each controller, along with the corresponding performance measures, are tabulated in Table 7.

$$\textbf{Maximum tracking error, MTE} = \textbf{Max}|\mathbf{e(t)}| \tag{16}$$

$$\textbf{Root mean square error, RMSE} = \sqrt{\frac{1}{n}\sum_{i=1}^{N}[e(t_i)]^2} \tag{17}$$

Figure 6 shows the output of each PID+F_{SS}, NH-PID+F_{SS}, and T-NPID+SIFLC+F_{GMS}, respectively, in response to the trajectory sine wave

input. Visually observed, the tracking performance is not observable, but the tracking errors presented are significantly noticeable. The error analysis improvement is reflected in Table 8. It is expected that the base PID controller will perform inadequately due to the mismatch between a linear controller and a nonlinear plant, resulting in a significant error. NH-PID and T-NPID+SIFLC perform exceptionally well, as the MTE is reduced drastically from the base controller. The formulation of the controller gains, which increase when the error increases, caters well to trajectory performance, particularly when the errors are significant during the peak amplitude of the sine wave.

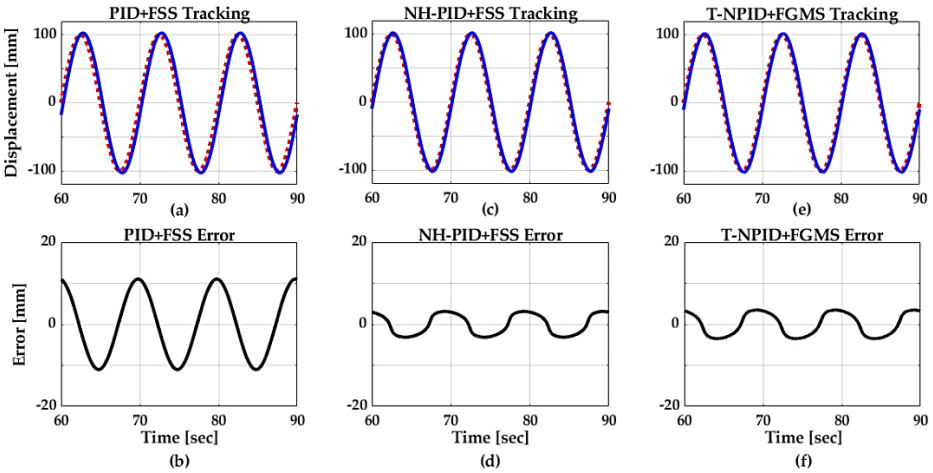

Figure 6: Simulation results for (a) PID+F_{SS} tracking, (b) PID+F_{SS} error, (c) NH-PID+F_{SS} tracking, (d) NH-PID+F_{SS} error, (e) T-NPID+SIFLC+F_{GMS} tracking, and (f) T-NPID+SIFLC+F_{GMS} error

T-NPID+SIFLC is able to reduce the MTE from 7.488 mm to 2.844 mm. NH-PID is between 3.131 mm. The T-NPID control strategy processes each error from the PID element (proportional error, integral error, and derivative error) accordingly. In contrast, the NH-PID processes the error in a lump-sum process only once. During the stability analysis using the Popov stability criterion [12], each PID component has a different maximum allowable gain, and the T-NPID is bounded by the condition [20], allowing it to perform better. The RMSE result mirrors the MTE as the accumulated error. RMSE decreases from 3.717 mm to 1.762 mm for NH-PID, and 1.563 mm for T-NPID+SIFLC.

Table 7: Simulation results for MTE and RMSE for all control strategies

Error Parameter	PID +F_{SS}	NH-PID +F_{SS}	T-NPID+SIFLC +F_{GMS}
MTE (mm)	7.488	3.131	2.844
RMSE (mm)	3.717	1.762	1.563

Figure 7 shows the experimental validation of each control strategy. It is observable that noises from the sensors and vibration are shown in the figure. Nevertheless, T-NPID+SIFLC performs the best, suppressing the errors the most.

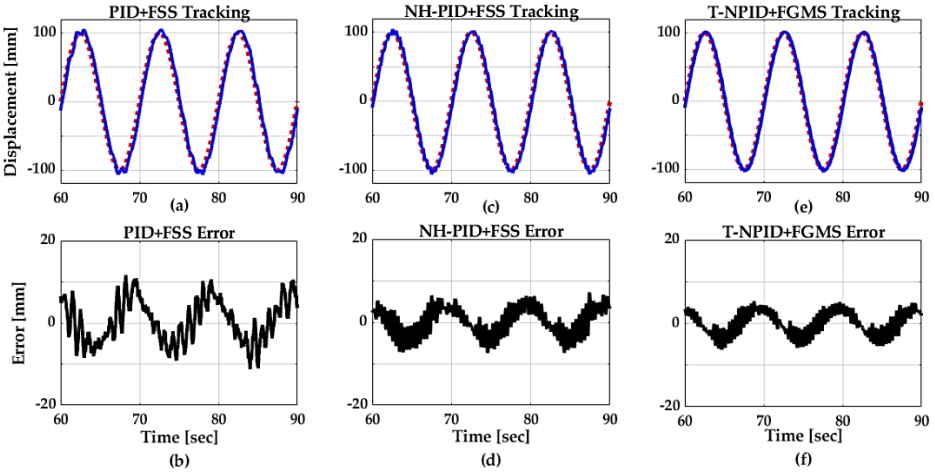

Figure 7: Experimental results for (a) PID+F_{SS} tracking, (b) PID+F_{SS} error, (c) NH-PID+F_{SS} tracking, (d) NH-PID+F_{SS} error, (e) T-NPID+SIFLC+F_{GMS} tracking, and (f) T-NPID+SIFLC+F_{GMS} error

Table 8: Experimental results for MTE and RMSE for all control strategies

Error Parameter	PID +F_{SS}	NH-PID +F_{SS}	T-NPID+SIFLC +F_{GMS}
MTE (mm)	12.54	7.147	6.416
RMSE	3.772	2.323	1.975

The improvement gains of each control strategy based on the experimental performance measure are tabulated in Table 9. NH-PID and T-NPID improved by 43.01% and 48.84%, respectively, compared to the classical PID, while the RMSE improved by 38.41% and 47.64%, respectively.

Table 9: Percentage improvement gains over PID+F_{SS}

Performance parameter	Percentage performance parameter improvement		
	PID +F_{SS}	NH-PID +F_{SS}	T-NPID+SIFLC +F_{GMS}
MTE (%)	-Ref-	43.01	48.84
RMSE (%)	-Ref-	38.41	47.64

The robustness test is based on 1 kg, 5 kg, and 9 kg additional loading to the plant. The highest available external load disturbance is 9 kg, limited by the hardware's capabilities. PID and NH-PID are only able to withstand the additional disturbance of up to 1 kg. After 1 kg, the system becomes unstable with high-frequency (HF) oscillations. T-NPID+SIFLC is able to withstand a maximum of 9 kg, as Table 10 tabulates the performance measure.

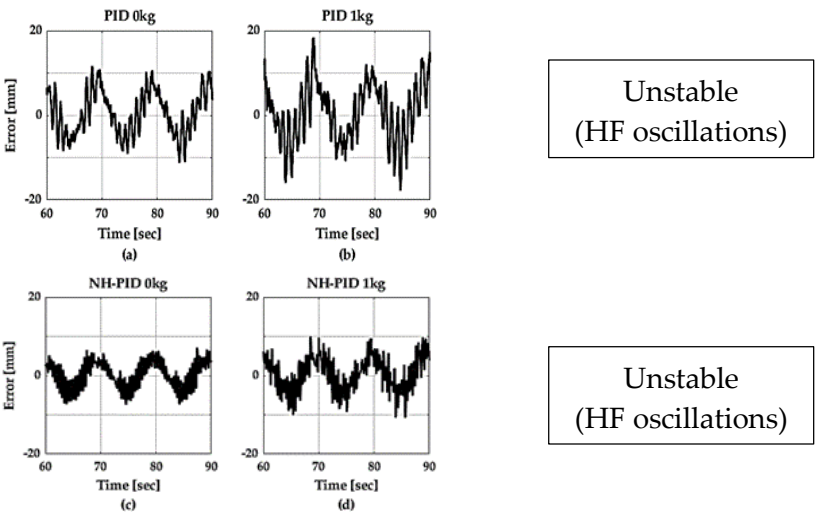

Figure 9: Errors for robust test (a) PID+F_{SS} 0 kg, (b) PID+F_{SS} 1 kg, (c) NH-PID+F_{SS} 0 kg, and (d) NH-PID+F_{SS} 1kg

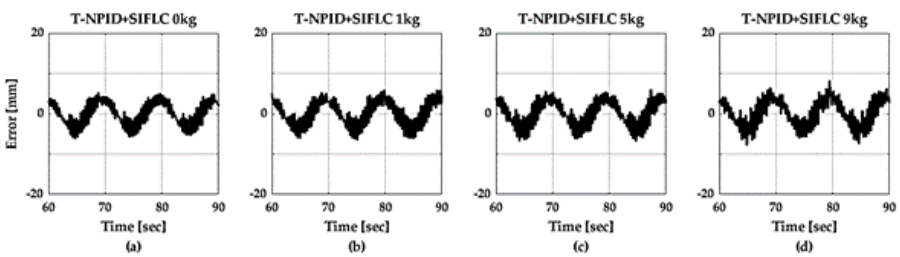

Figure 10: Errors for robust test (a) T-NPID+SIFLC+F_{GMS} 0 kg, (b) 1 kg, (c) 5 kg, and (d) 9 kg

The SIFLC module enhances the system's adaptability in response to additional external disturbances. NH-PID increases the gains when the error increases, and therefore, the system becomes aggressive to overcome the error. Adaptation of SIFLC reduces aggressiveness by varying the nonlinear gains based on the error and the membership functions during the design process. In the design, precautions are necessary when the parameter (g) is reduced excessively (loosened), as the accuracy of the strategy can be compromised. The same concept of variable gain rate has been presented previously by the same author in [9] and [21], where the gain rate is controlled by a classical fuzzy logic. Robustness for sine wave tracking has been experimentally tested up to 17 kg, as shown in Figure 11. This research aligns with previous studies by varying the nonlinear gains or gain, which enables the strategy to become more robust.

Table 10: Robustness test with external load disturbance

Additional load	PID +F_{SS}		NH-PID +F_{SS}		T-NPID+SIFLC +F_{GMS}	
1 kg	MTE	18.43	MTE	10.42	MTE	6.683
	RMSE	4.949	RMSE	4.585	RMSE	2.121
5 kg	Unstable (HF oscillations)		Unstable (HF oscillations)		MTE	6.924
					RMSE	2.187
9 kg	Unstable (HF oscillations)		Unstable (HF oscillations)		MTE	8.305
					RMSE	2.342

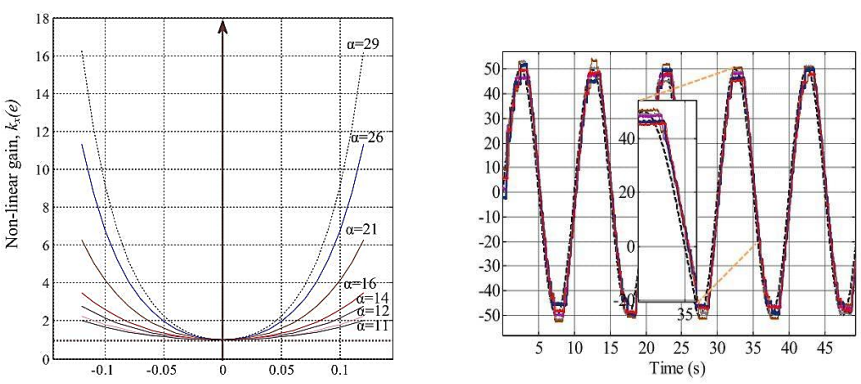

(a) (b)

Figure 11: MN-PID, robust nonlinear PID by [21] (a), multi-rate α for the nonlinear function and (b) robustness sinewave experimental test

5.0 CONCLUSION

The development and analysis of the T-NPID+SIFL+F_{GMS} control strategy demonstrate its effectiveness in achieving both a more precise trajectory and robust performan**ce** in servo pneumatic actuators. Lyapunov's asymptotic tracking analysis confirms the convergence of each strategy to zero error, where the NH-PID+F_{ss} and T-NPID+SIFLC+F_{GMS} outperform the classical PID controller from the results of the eigenvalues. In simulation and experimental tracking performances, it is confirmed that the final and novel controller, T-NPID+SIFLC+F_{GMS}, performs the best, with the lowest MTE and RMSE, respectively. Where the PID and NH-PID are able to withstand only 0 kg and 1 kg, the final T-NPID+SIFLC is able to withstand the maximum available up to 9 kg of external load disturbance. An additional smooth trajectory, such as multiple level S-curves, will able to consolidate the robustness and tracking performance. Additionally, an in-depth comparison of the friction compensation module F_{GMS} and the F_{SS} will facilitate a deeper discussion of the friction compensation effect on the entire control strategy.

ACKNOWLEDGMENTS

The authors would like to acknowledge the financial support provided by the Ministry of Higher Education (MOHE) of Malaysia through the Fundamental Research Grant Scheme (FRGS), No: FRGS/1/2020/TK0/UTEM/02/33, and Universiti Teknikal Malaysia Melaka (UTeM), with reference number FRGS/1/2020/FKP-COSSID/F00444.

AUTHOR CONTRIBUTIONS

K.N. Kamaludin: Conceptualization, Methodology, Writing- Original Draft Preparation; L. Abdullah: Validation, Supervision, Writing-Reviewing; S.N.S. Salim: Writing-Reviewing; A.S.N. Chairat: Data Collection, Result and Validation.

CONFLICTS OF INTEREST

The manuscript has not been published elsewhere and is not under consideration by other journals. All authors have approved the manuscript, agree with its submission and declare no conflict of interest on the manuscript.

REFERENCES

[1] P. Joji, *Pneumatic Controls*. India: Wiley India, 2008.

[2] S. Dudić, V. Reljić, D. Šešlija, N. Dakić, and V. Blagojević, "Improving energy efficiency of flexible pneumatic systems", *Energies*, vol. 14, no. 7, 2021.

[3] D. Saravanakumar and B. Mohan, "Nonlinear mathematical modelling of servo pneumatic positioning system", *Applied Mechanics and Materials*, vol. 313, pp. 962–966, 2013.

[4] D. Meng, G. Tao, H. Liu, and X. Zhu, "Adaptive robust motion trajectory tracking control of pneumatic cylinders with lugre model-based friction compensation", *Chinese Journal of Mechanical Engineering (English Edition)*, vol. 27, no. 4, pp. 802–815, 2014.

[5] X. B. Tran, V. L. Nguyen, N. C. Nguyen, D. T. Pham, and V. L. Phan, "Sliding mode control for a pneumatic servo system with friction compensation", *Advances in Engineering Research and Application*, vol. 104, pp. 648–656, 2019.

[6] F. Soleymani, S. M. Rezaei, S. Sharifi, and M. Zareinejad, "Position control of a servo-pneumatic actuator using Generalized Maxwell-Slip friction model", in *2016 4th International Conference on Robotics and Mechatronics*. Tehran, Iran: IEEE, 2016, pp. 246–251.

[7] R. P. Borase, D. K. Maghade, S. Y. Sondkar, and S. N. Pawar, "A review of PID control, tuning methods and applications", *International Journal of Dynamics and Control*, vol. 9, no. 2, pp. 818–827, 2021.

[8] S. Bennett, *A History of Control Engineering 1930-1955*. London, United Kingdom: Peter Peregrinus Ltd., 1993.

[9] S. N. S. Salim, "Modeling and control design of an industrial pneumatic actuator system," Ph.D. dissertation, Universiti Teknologi Malaysia, Skudai, Johor, 2014.

[10] L. Abdullah, Z. Jamaludin, Chiew T.H, N.A. Rafan and M.Y. Yuhazri, "Extensive tracking performance analysis of classical feedback control for XY stage ballscrew drive system", *Applied Mechanics and Materials*, vol. *229*, pp. 750-755, 2012.

[11] G. Filo, "A review of Fuzzy Logic method development in hydraulic and

pneumatic systems", *Multidisciplinary Digital Publishing Institute*, vol. 16, no. 2(2), 2023.

[12] S. C. K. Junoh, S. N. S. Salim, L. Abdullah, N. A. Anang, T. H. Chiew, and Z. Retas, "Nonlinear PID triple hyperbolic controller design for XY table ball-screw drive system", *International Journal of Mechanical and Mechatronics Engineering*, vol. 17, no. 3, pp. 1–10, 2017.

[13] K. N. Kamaludin, L. Abdullah, S. N. S. Salim, "Performance evaluation of an adaptive sigmoid friction compensation for pneumatic trajectory," in *2023 8th International Conference on Control and Robotics Engineering*, Niigata, Japan: IEEE, 2023, pp. 165-171.

[14] S. N. S. Salim, S. C. K. Junoh, L. Abdullah, and Z. Retas, "NPID double hyperbolic controller with particle swarm optimization (PSO) technique for XY table ballscrew drive system", *Journal of Advance Manufacturing Technology*, vol. 14, no. 2, pp. 41-52, 2020.

[15] B.-J. Choi, S.-W. Kwak, and B. K. Kim B, "Design of a single-input fuzzy logic controller and its properties", *Fuzzy Sets and Systems*, vol. 106, no. 3, pp. 299–308, 1999.

[16] F. Taeed, Z. Salam, and S. Ayob, "FPGA implementation of a single-input fuzzy logic controller for boost converter with the absence of an external Analog-to-Digital converter", *IEEE Transactions on Industrial Electronics*, vol. 59, no. 2, pp. 1208–1217, 2012.

[17] Z. Salam, F. Taeed, and S. M. Ayob, "Design and implementation of a single input Fuzzy Logic controller for boost converters", *Journal of Power Electronics*, vol. 11, no. 4, pp. 542-550, 2011.

[18] R. M. Murray, Z. Li, and S. S. Sastry, *A mathematical introduction to robotic manipulation*. Boca Raton: CRC Press, 1994.

[19] R. C. Dorf and R. H. Bishop, *Modern control systems*. Prentice Hall, 2011

[20] H. Seraji, "A New Class of Nonlinear PID Controllers with Robotic Applications", *Journal of Robotic Systems*, vol. 15, no. 3, pp. 161-181, 1998.

[21] S. N. S. Salim, M. F. Rahmat, A. A. M. Faudzi, and Z. H. Ismail, "Position control of pneumatic actuator using an enhancement of NPID controller based on the characteristic of rate variation nonlinear gain", *International Journal of Advanced Manufacturing Technology*, vol. 75, no. 1–4, pp. 181–195, 2014.